Surface Science 629 (2014) 35–40

Contents lists available at ScienceDirect

Surface Science

journal homepage: www.elsevier.com/locate/susc

Contributions of dispersion forces to R-3-methylcyclohexanone physisorption on low and high Miller index Cu surfaces

Daniel S. Wei [a], Bharat S. Mhatre [b], Andrew J. Gellman [b], David S. Sholl [a,*]

[a] School of Chemical & Biomolecular Engineering, Georgia Institute of Technology, 311 Ferst Drive NW, Atlanta, GA 30332, USA
[b] Department of Chemical Engineering, Carnegie Mellon University, 5000 Forbes Avenue, Pittsburgh, PA 15213, USA

ARTICLE INFO

Available online 25 March 2014

Keywords:
Density functional theory
Physisorption
Temperature programmed desorption

ABSTRACT

The physisorption of R-3-methylcyclohexanone on low and high Miller index Cu surfaces is studied with temperature programmed desorption (TPD) and density functional theory (DFT). The DFT calculations are performed with D2, vdW-optB86b, and vdW-optB88 dispersion corrected methods. The adsorption energies calculated by the dispersion corrected methods are more comparable to the TPD results than those calculated without dispersion corrections, although, the former methods have a tendency to overbind the surface adsorbates. The implementation of dispersion corrected methods also indicates a possible adsorbate induced surface reconstruction on Cu(110).

1. Introduction

Kohn–Sham Density functional theory (KS-DFT) is an important tool in the study of surface–adsorbate interactions [1,2]. Using the local density approximation (LDA) or the generalized gradient approximation (GGA) functional, DFT is able to predict adequately the behavior of atoms or small chemisorbed species on metal surfaces. However, as adsorbate size increases, weak dispersion forces become significant for many physisorbed species. Neither LDA nor GGA can correctly describe these dispersion forces [3,4]. Grimme sought to address these drawbacks with the introduction of a semi-empirical dispersion force correction to the GGA functional [5,6]. Soler and others also tried to account for the dispersion forces by using non-local van der Waals density functionals [7,8]. The optimized B86b method uses a new gradient-corrected exchange energy to account for interaction in systems with large density gradient [9,10]. The optimized B88 method further improves this through a proper asymptotic potential for the gradient-corrected exchange energy approximation [4,11,12]. These dispersion corrected methods have been shown to significantly increase the adsorption energies calculated using DFT and improve agreement with experimental data [13–17]. Peköz et al. reported that the adsorption energy of dichlorobenzene on Au and Pt surfaces increased from the negligible value of 0.1 eV to 1.0–1.1 eV after correcting the conventional GGA with the vdW-DFT method [18]. A study of benzene, thiophene, and pyridine adsorption on Au(111) and Cu(111) by Tonigold and Gross achieved better agreement with experimental data using DFT-D than when using the nonhybrid GGA, although, their calculations also revealed a tendency of DFT-D to overbind adsorbates to metal substrates [19].

The emergence of dispersion force corrections to DFT methods has allowed us to reexamine interesting adsorbates for which physisorption forces are expected to contribute significantly to adsorption. One such interaction is the enantioselective adsorption of chiral hydrocarbons on naturally chiral surfaces [20–24]. Temperature-programmed desorption (TPD) has revealed measurable enantiospecific differences in the desorption energies of enantiomers such as 3-methylcyclohexanone and propylene oxide from chiral Cu surfaces [25–29]. Those studies examined intrinsically chiral Cu single crystal surfaces created by cleaving normal to a low symmetry direction of the achiral FCC crystal [30–32]. The adsorption and desorption of R-3-methylcyclohexanone (R-3MCHO) have been studied on a large set of Cu single crystal surfaces that spans the stereographic triangle and includes the three low Miller index surfaces Cu(111), Cu(110) and Cu(100), six stepped surfaces Cu(221), Cu(771), Cu(533), Cu(511), Cu(410) and Cu(430), and seven kinked surfaces $Cu(643)^{R\&S}$, $Cu(653)^{R\&S}$, $Cu(17,5,1)^{R\&S}$, $Cu(13, 9, 1)^{R\&S}$, $Cu(821)^{R\&S}$, $Cu(651)^{R\&S}$, and $Cu(531)^{R\&S}$. Cu(*hkl*) surfaces that have $h \neq k \neq l$ and $h \cdot k \cdot l \neq 0$ are intrinsically chiral and exist in two enantiomorphic forms denoted as $(hkl)^R$ and $(hkl)^S$. TPD results show that the desorption energies, ΔE_{des}, of R-3MCHO from the terraces are roughly equivalent on all surfaces, as are the desorption energies from the step sites and the kink sites. Not surprisingly, the trend among the desorption energies is $\Delta E_{des}^{terr} < \Delta E_{des}^{step} < \Delta E_{des}^{kink}$. However, on the enantiomorphs of the chiral surfaces there are measurable enantiospecific differences of ~1 kJ/mol in the desorption energies from the enantiomorphous kinks: $\Delta E_{des}^{R-kink} \neq \Delta E_{des}^{S-kink}$. Using the PW-91 functional, DFT simulation of the adsorption energy of R-3MCHO from Cu(111) and Cu(322) yielded values that were ~0.45 eV

* Corresponding author.
E-mail addresses: daniel.wei@chbe.gatech.edu (D.S. Wei), bmhatre@andrew.cmu.edu (B.S. Mhatre), gellman@cmu.edu (A.J. Gellman), david.sholl@chbe.gatech.edu (D.S. Sholl).

http://dx.doi.org/10.1016/j.susc.2014.03.022
0039-6028/

lower than the experimental values [33]. This discrepancy was attributed to PW91's inability to account for dispersion contributions to the binding of R-3MCHO to the Cu surfaces. A similar study using the non-hybrid PBE functional estimated the benzene desorption energy on Cu(111) to be −0.06 eV [34], but experiments estimate the adsorption energy between −0.53 and −0.62 eV [35,36]. Here we use R-3MCHO adsorption on Cu surfaces as a benchmark test for several dispersion corrected DFT methods. This study utilizes DFT and TPD to quantify the effectiveness of various dispersion force corrected methods for predicting surface–adsorbate interaction by examining R-3MCHO physisorption behavior on the low and high Miller index Cu surfaces.

2. Methods

2.1. Density functional theory

Periodic DFT calculations were conducted with the Vienna *Ab initio* Simulation Package (VASP) [37–40]. The electron–electron exchange and correlation interactions were described with the PBE-GGA functional [41,42]. Core–electron interactions were modeled with the projector augmented-wave (PAW) potential [43,44]. All calculations used a plane wave expansion cutoff of 500 eV. Structural optimization was performed by a conjugate gradient algorithm with a force stopping criterion of 0.03 eV/Å. The study utilized Grimme's D2 (PBE-D2), the vdW_optB86b (PBE-B86b), and the vdW_optB88 (PBE-B88) dispersion corrected methods [6,12]. Bulk Cu atoms were examined with 8 Cu atoms in an FCC lattice using 16 × 16 × 16 k-points. The atomic positions, unit cell shape, and unit cell size were allowed to relax for each dispersion corrected method. The lattice constants are reported in Table 1. The Cu lattice constants predicted by PBE-D2, PBE-B86b, and PBE-B88 were found to be 1.74%, 0.85%, and 0.10% smaller, respectively, than the lattice constant calculated by PBE-GGA. All surface calculations were performed using the optimized lattice constant determined using the functional used in that calculation.

All surface calculations had a vacuum spacing of at least 10 Å. The required slab thickness was determined with R-3MCHO adsorption on Cu(111). The minimum thickness was achieved when the presence of an additional layer changed the R-3MCHO adsorption energy by less than 0.05 eV. This was determined to be three Cu(111) layers with the bottommost layer immobilized. Unless otherwise stated, surfaces were modeled as an approximately 7 Å thick slab with the bottommost 3 Å immobilized. Molecules were only adsorbed on one side of the slab. The low Miller index Cu(111), Cu(100), and Cu(110) surfaces were made up of $p(5 \times 5)$ surface unit cells and were examined with 3 × 3 × 1 k-points. The stepped Cu(221) and Cu(322) surfaces were modeled with $p(2 \times 6)$ surface unit cells. The kinked Cu(643)^R consisted of only one surface unit cell. Calculations for the latter three surfaces used 2 × 2 × 1 k-points. The resolution in *k*-points were chosen to ensure good convergence while reducing computational cost. Table 2 below demonstrated that these *k*-points offer sufficient convergence for our study.

Calculations were also performed for a reconstructed Cu(110) surface to mimic the (2 × 1) missing-row reconstruction seen for Pt(110) [45–47]. The (2 × 1) reconstructed Cu(110) surface was modeled with a slab approximately 10 Å thick with the bottommost 5 Å immobilized. The reconstructed Cu(110) supercell had a $p(2 \times 5)$ surface unit cell and used 2 × 2 × 1 k-points. A single R-3MCHO was placed on each computational supercell to simulate adsorption. The isolated R-3MCHO molecule in a 20 × 20 × 20 Å cell was sampled only at the Γ point. Various geometric configurations were examined, and the lowest energy state was used as the reference state. On the clean surface, the adsorption energy was defined as,

Table 1
Bulk Cu lattice for each dispersion corrected method.

Functional	Lattice
PBE-GGA	3.63
PBE-D2	3.57
PBE-B86b	3.60
PBE-B88	3.63

Table 2
The total adsorption energy of R-3MCHO per unit cell on different surfaces as a functional of resolution in *k*-points.

	Cu(111)	Cu(100)	Cu(110)	Cu(221)	Cu(643)^R
1 × 1 × 1	−1.16	−1.20	−1.22	−1.40	−1.58
2 × 2 × 1	−1.02	−1.18	−1.14	−1.50	−1.49
3 × 3 × 1	−1.05	−1.17	−1.17	−1.44	−1.51
4 × 4 × 1	−1.04	−1.18	−1.15	−1.46	−1.52

$$\Delta E_{\text{Adsorption}} = E_{\text{total}} - E_{\text{3MCHO}} - E_{\text{Surface}} \quad (1)$$

where E_{total}, E_{3MCHO}, E_{Surface} are the total energy of the relaxed structure including the adsorbed molecule, the energy of the isolated R-3MCHO, and the clean surface energy, respectively. For the reconstructed surface, the adsorption energy had to account for the energy lost to the reconstruction. The effective adsorption energy was defined as,

$$\Delta E_{\text{Effective adsorption}} = E_{\text{total}} - E_{\text{3MCHO}} - E_{\text{Reconstructed surface}} - A^{*}\Delta E_{\text{Reconstruction}} \quad (2)$$

where $E_{\text{Reconstructed surface}}$ is the total energy of the clean reconstructed surface, A is the reconstructed surface area, and $\Delta E_{\text{Reconstruction}}$ is the energy required to reconstruct 1 Å^2 of the surface. A negative $\Delta E_{\text{Reconstruction}}$ denoted an unfavorable reconstruction as the surface required energy from the environment to undergo reconstruction.

Multiple preferred adsorption configurations and location combinations were systematically examined for each surface. A list of possible adsorption geometries for each surface was generated by placing oxygen on a large number of possible high symmetry surface sites and allowing the methylcyclohexane group to rotate around the oxygen. On high Miller index surface, special attention was paid to examine geometries where the methylcyclohexane group was on top of the stepped or kinked sites. Typically, these initial geometries converged to a few selective local minima, and only the most energetically preferred states were used in this study.

2.2. TPD experimental methods

TPD has been used to measure the influence of surface structure on the desorption energies of R-3MCHO from a large set of Cu(*hkl*) single crystal surfaces and under ultra-high vacuum (UHV) conditions. Details of the experimental measurements can be found in prior publications [26,28,48,49]. Briefly, the single crystal surfaces were cleaned in UHV by cycles of Ar^+ ion sputtering and annealing at temperatures in the range 800–1000 K. The orientation and the crystallinity of the surfaces were examined using low energy electron diffraction. Once the Cu surfaces were clean, R-3MCHO was adsorbed at temperatures of ~170 K by exposure of the surfaces to vapor introduced into the UHV chamber through a leak valve. The adsorption temperature of 170 K limited the coverage to one monolayer and prevented the formation of condensed multilayers. TPD of the adsorbed monolayer was performed by positioning the Cu single crystal in front of the aperture to a mass spectrometer and heating the crystal at 1 K/s while monitoring the signal at m/q = 39 amu.

3. Results and discussions

3.1. TPD data

One of the important features of R-3MCHO adsorption on the single crystal Cu surfaces is that its binding energy is very sensitive to the local structure of the adsorption site. As a consequence, the desorption temperature in a TPD experiment is indicative of the local structure of the site from which the R-3MCHO desorbed [26,28,48–51]. The data in Fig. 1 show the TPD spectra obtained from saturated monolayer of R-3MCHO adsorbed on the Cu(111), Cu(100), Cu(110), Cu(221), and $Cu(643)^R$ surfaces. In the classification system of Jenkins et al. the Cu(111) and Cu(100) surfaces are considered flat because they have close packed rows of atoms running in two or more directions across the surfaces [52]. The desorption of R-3MCHO from flat Cu terraces occurs at ~230 K. The Cu(110) and Cu(221) surfaces are considered to be stepped because they have close packed rows running in one direction across the surface. R-3MCHO desorption occurs at ~345 K from these steps. Using the microfacet framework of van Hove and Somorjai, the $Cu(643)^R$ structure has a (111) terrace, (100) step edge, and a (110) kink [53]. The R-3MCHO TPD spectrum from the $Cu(643)^R$ surface exhibits three resolved desorption features at 230, 345, and 385 K that can readily be assigned to desorption from flat terraces, steps and kinks, respectively [26,50,51]. Enantiospecific adsorption on the $Cu(643)^{R\&S}$ surfaces is revealed by a ~3.5 K difference (not shown) in desorption temperatures from the two enantiomorphous surfaces [26,50,51].

The adsorption energies of R-3MCHO on the Cu surfaces are determined from the peak desorption temperatures. Following the Redhead method for first order desorption [54], we calculated the adsorption energy from the peak desorption temperature using

$$E_d/RT_P^2 = \nu/\beta^* \exp\left(-E_d/RT_p\right) \quad (3)$$

where $E_d = -E_a$ is the measured desorption energy, R is the gas constant, T_P is the peak desorption temperature in Kelvin, ν is the pre-factor, and β is the heating rate. In all cases, $\beta = 1$ K/s and we assumed $\nu = 10^{18}\ s^{-1}$ [55]. This analysis assumes that the adsorption energy is independent of surface coverage on each surface and that ν is constant for R-3MCHO desorption from all Cu surfaces. The peak desorption temperature for each Cu surfaces and the resulting adsorption energies are listed in Table 3.

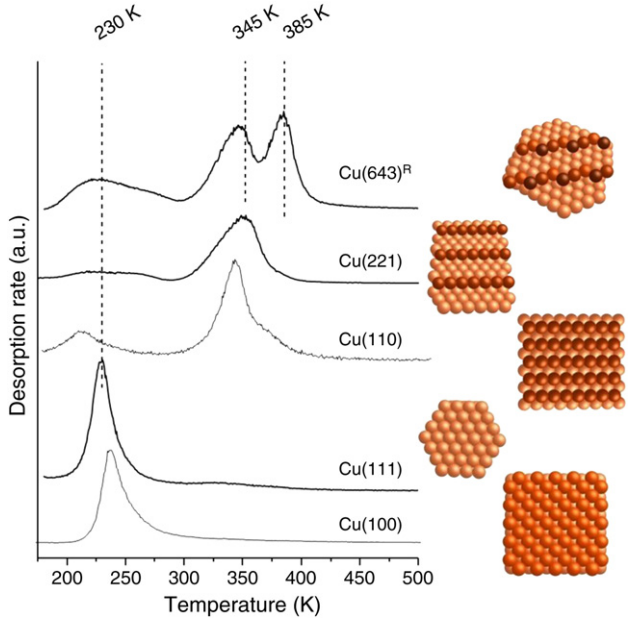

Fig. 1. TPD of R-3MCHO on various Cu surfaces. The peak temperatures for desorption from the flat terraces, the steps and the kinks are ~230, ~345, and ~385 K, respectively. Insets to the right show the ideal structure of each surface, with color coding used to indicate the coordination number of surface atoms.

Table 3
Adsorption energy (E_a) of R-3MCHO on Cu surfaces.

Surface	Peak T (K)	E_a (eV)
Cu(111)	230	−0.85
Cu(100)	235	−0.87
Cu(110)	335	−1.26
Cu(221)	348	−1.31
$Cu(643)^R$	385	−1.45

While the pre-factor ν is not exact, the adsorption energies are only weakly sensitive to changes in the pre-factor values. If ν is lowered by an order of magnitude, the adsorption energy on $Cu(643)^R$ in Table 3 changes to −1.37 eV, a decrease of less than 5%. This difference impacts neither the analysis nor the conclusions of this work. The lower temperature desorption peaks on $Cu(643)^R$ were attributed to desorption from the flat terrace and straight steps that were created through surface roughening [49].

3.2. Adsorption on low Miller index Cu surfaces

Fig. 2 illustrates the adsorption geometries of R-3MCHO on low Miller index Cu surfaces, as calculated by DFT-D2. The carbonyl group binds between two adjacent surface Cu atoms. The cyclohexane ring adopts the chair formation with the methyl group in an equatorial position, and the ring lies flat on the surface with a slight tilt towards the methyl group. Similar geometries were observed on Cu(110) and Cu(100). The dominant role of the carbonyl group in binding the R-3MCHO to the surface is consistent with the large frequency shifts observed in the FTIR spectra of R-3MCHO on the $Cu(643)^{R\&S}$ surfaces [27].

The experimental and DFT calculated R-3MCHO adsorption energies on the low Miller index Cu surfaces are given in Table 4. The PBE functional underestimated the adsorption energy of R-3MCHO by 0.56–0.85 eV/adsorbate on these Cu surfaces. This result is similar to that of Bhatia and Sholl, who reported a 0.45 eV/adsorbate underestimation of the R-3MCHO adsorption energy on Cu(111) using the PW-91 functional [33]. It is also consistent with McNellis et al., who reported a 0.55 eV/adsorbate underestimation of the adsorption energy of benzene on Cu(111) with the PBE functional [34]. The dispersion corrected methods, summarized in Table 4, overestimated the adsorption energy of R-3MCHO on the low index Cu surfaces by 0.06–0.32 eV/adsorbate. Similar overbinding of adsorption has been reported by Grimme et al. [13]. We also calculated the dispersion contributions to the adsorption energy by subtracting the PBE-GGA based adsorption energy from each of the dispersion corrected methods. Table 5 shows the dispersion contribution to total adsorption energy and as a fraction of the total adsorption energy for each method. The large dispersion contributions are consistent with a physisorbed molecule. The variations in dispersion contributions among the surfaces were correlated with the atomic densities of the different surfaces: Cu(111) > Cu(100) > Cu(110). We also reported the distance between the plane of the surface Cu atom and the center of the cyclohexane ring for R-3MCHO on Cu(111) in Table 4. The calculated heights for the dispersion corrected methods were similar to the value of 3.6 Å reported by Witte et al., for cyclohexane binding above Cu(111) [56]. In that work, the inclusion of the dispersion forces brought the cyclohexane ring closer to the Cu(111) surface by 0.14–0.32 Å, depending upon which correction method was used. Compared to the other two dispersion correction methods, the

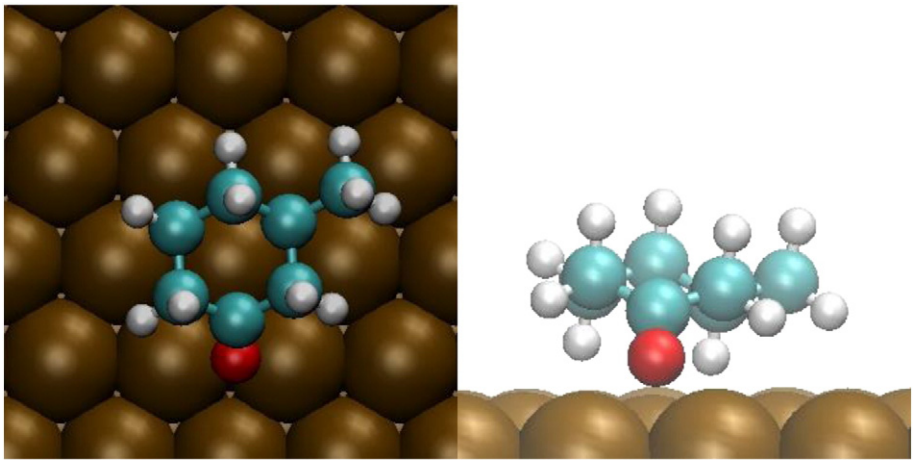

Fig. 2. Adsorption geometry of 3MCHO on Cu(111), as calculated with DFT using the PBE-D2 functional.

shorter distance predicted using PBE-D2 also points to its stronger overbinding of the adsorbate.

On the surfaces listed in Table 4, the PBE functional predicts the strongest binding to the Cu(110) surface followed by binding on Cu(100) and then on Cu(111). The carbonyl group preference for binding to the less coordinated surface Cu atoms probably contributed to this ordering of adsorption strengths. The dispersion corrected methods all predicted similar adsorption energies on Cu(100) and Cu(110), which was not consistent with our TPD observations. The experimental results show that the R-3MCHO binds most strongly to Cu(110), and that the adsorption energy on Cu(100) is roughly equal to that on Cu(111). In section 3.4, we attempted to address this shortcoming by considering a possible surface reconstruction of Cu(110). While the PBE-B88 method provided the most accurate adsorption energies, the improvement over the other methods was not significant. Since the Grimme method does not account for screening in the sea of electrons, the method may be regarded as less accurate on metal surfaces. Preliminary calculations, however, did not indicate a clear disadvantage to this method as compared to PBE-B86b and PBE-B88. Because our study was focused on examining the adsorption energy differences of R-3MCHO on other Cu surfaces, the inaccuracy due to screening would affect all surfaces similarly and lessen the impact on overall results. With these observations, we reduced calculation complexity for the remaining results described below by employing only the PBE-D2 dispersion corrected method to examine adsorption of R-3MCHO on the Cu(221) and Cu(643) surfaces.

3.3. R-3MCHO adsorption on high Miller index Cu surfaces

Our study also probed the ability of dispersion corrected DFT methods to describe the differences in R-3MCHO adsorption energies on low and high Miller index Cu surfaces. Earlier calculations have indicated a distinct increase in adsorption energy from low to high Miller index surfaces. The adsorption geometries of R-3MCHO on the straight steps and kinked step edge are illustrated in Fig. 3. On both Cu(221) and Cu(643)^R, the carbonyl group binds between Cu atoms in the straight step edge. Similar to its adsorption on low Miller index surfaces, the cyclohexane ring adopted a chair conformation. The ring lies flat against the terrace with a tilt towards the methyl group. Due to the presence of the kinked step edge, the tilt was more pronounced on Cu(643)^R.

The calculation using the PBE-D2 functional overbinds R-3MCHO on Cu(221) and Cu(643)^R as on Cu(111). The TPD data indicated adsorption energies of −1.31 eV and −1.45 eV on Cu(221) and Cu(643)^R, respectively, while the PBE-D2 calculation predicted the adsorption energies of −1.50 eV and −1.55 eV on the same two surfaces. On Cu(221), R-3MCHO adsorbed along the bottom of the step with the oxygen atom sitting between two adjacent Cu atoms in the step edge. The cyclohexane ring lies parallel to the terrace, and the side with the methyl group leans towards the terrace. On Cu(643)^R, the oxygen atom sits within the kinked site bound between two adjacent atoms in the straight step edge while the cyclohexane ring tilts away from the kink site. Fig. 4 shows the differences between the adsorption energy on Cu(111) and the adsorption energies on Cu(221), Cu(322), and Cu(643)^R. For each DFT-D method, the difference was calculated by subtracting the adsorption energy of R-3MCHO on Cu(111) from its adsorption energy on the other surfaces. Fig. 4 also compared our calculated difference to energy differences reported by Bhatia and Sholl [33] Both PBE and PBE-D2 show larger adsorption energy differences than the experimental values.

While our PBE calculated energy differences between Cu(111) and kinked Cu surface agreed with those reported by Bhatia and Sholl, our calculation showed a significantly different adsorption energy difference between Cu(111) and the stepped Cu surface. We attempted to understand this discrepancy by calculating the adsorption of R-3MCHO on Cu(322). The calculation indicated a difference of 0.28 eV between our calculated adsorption energy and those reported by Bhatia and Sholl [33]. Calculation on Cu(111) and Cu(221) using PW-91 also indicated an adsorption energy stronger than those reported by Bhatia and Sholl. The consistency of our calculated adsorption energy between Cu(221) and Cu(322) and the agreement between our calculated Cu(221) and the experimental TPD data suggest a possible inaccuracy

Table 4
Summary of R-3MCHO adsorption energies (eV) on the low Miller index Cu surfaces. Italic values in parenthesis are differences between calculated results and those estimated on the basis of TPD data.

	TPD	PBE-GGA	PBE-D2	PBE-B86b	PBE-B88
Cu(111)	−0.85	−0.15 (*0.70*)	−1.07 (*−0.22*)	−0.98 (*−0.13*)	−0.93 (*−0.08*)
Cu(100)	−0.87	−0.31 (*0.56*)	−1.19 (*−0.32*)	−1.20 (*−0.33*)	−1.15 (*−0.28*)
Cu(110)	−1.26	−0.41 (*0.85*)	−1.19 (*0.07*)	−1.21 (*0.05*)	−1.15 (*0.11*)
Height above Cu(111) (Å)		3.80	3.48	3.66	3.60

Table 5
Dispersion contribution to total adsorption energies (eV) for R-3MCHO adsorption on low Miller index Cu surfaces.

	PBE-D2	PBE-B86b	PBE-B88
Cu(111)	−0.92 (86%)	−0.83 (84%)	−0.78 (83%)
Cu(100)	−0.88 (74%)	−0.89 (74%)	−0.84 (73%)
Cu(110)	−0.78 (65%)	−0.80 (66%)	−0.74 (64%)

in the earlier result reported by Bhatia and Sholl. TPD indicated a larger adsorption energy difference of 0.11 eV between Cu(221) and Cu(643)^R than the difference predicted by our calculations. The PBE and PBE-D2 calculation showed a difference of only 0.03 eV and 0.06 eV between the two surfaces. While it is clear that dispersion corrected methods such as PBE-D2 can account for dispersion forces, they failed to calculate the absolute binding energies for the range of surface we studied due to the large overbinding of 3MCHO on Cu. Nonetheless, the method was able to achieve a useful comparison between adsorption on low and high Miller index Cu surfaces.

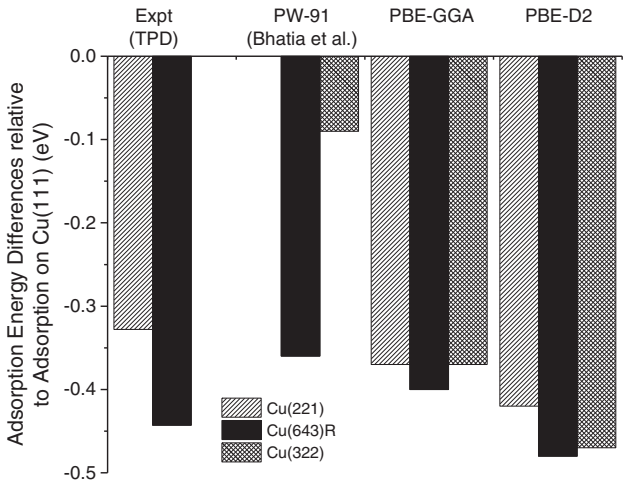

Fig. 4. R-3MCHO adsorption energy differences between Cu(111) and stepped/kinked Cu surfaces for TPD, PW-91[33], PBE-GGA, and PBE-D2.

3.4. Reconstruction of Cu(110)

We attempted to address the experimental and simulated adsorption energy discrepancy for R-3MCHO adsorption on Cu(100) and Cu(110). Reexamination of the TPD data in Fig. 1 shows the 3MCHO desorbs from Cu(110) at ~110 K above that of Cu(111) and Cu(100). The ~340 K desorption temperature on Cu(110) was much closer to the desorption temperature of 345 K observed for Cu(221). It was also similar to the desorption temperature of 3MCHO from the straight step of Cu(643)^R. This suggested that Cu(110) behaves more like a step edge than a flat terrace. STM and TPD study of R-3MCHO adsorption on Cu(533) and Cu(221) at elevated temperature showed an adsorbate induced reconstruction on these stepped edges [57]. We therefore investigated possible surface reconstructions in which Cu(110) was transformed into a more stepped surface. FCC Pt naturally undergoes a (2×1) missing row reconstruction where every other row of the (110) ridge is removed [46,47,58]. Furthermore, Raval et al. reported that the adsorption on CO induced a (2×1) missing row reconstruction on the Pd(110) [59]. While Cu(110) does not undergo this reconstruction naturally, the study used this simple reconstruction to test our hypothesis. R-3MCHO was found to have an adsorption energy of −1.55 eV on the (2×1) missing row reconstructed Cu(110). Accounting for the energy required for the surface reconstruction, the R-3MCHO has an effective adsorption energy of −1.37 eV with respect to clean unreconstructed Cu(110). As shown in Fig. 5, the calculated effective adsorption energy of 3MCHO on the reconstructed Cu(110) surface also overbinds the adsorbate to the surface. This overbinding was consistent with what we have observed on the other Cu surfaces.

While it did not give the correct absolute binding energy, the reconstructed Cu(110) achieved a better agreement with the trends of adsorption energy observed in experimental study for the different surfaces. The presence of the consistent overbinding was also consistent with observation made on R-3MCHO adsorption on different Cu surfaces, and it helped to support the hypothesis of a possible adsorbate induced surface reconstruction on Cu(110). Additional studies will be necessary to determine the exact mechanism and structure of this reconstruction.

4. Summary

The study examined three different dispersion corrected DFT methods to model R-3MCHO adsorption on low Miller index Cu surfaces. All three methods show an overbinding of R-3MCHO to the surface to varying degrees, and none of them was able to achieve a quantitative agreement with TPD results. While PBE-B88 performed better than PBE-D2 and PBE-B86, the overall improvement was small. Adsorption calculations on the stepped Cu(221) and the kinked Cu(643)^R using PBE-D2 indicated a similar overbinding of R-3MCHO.

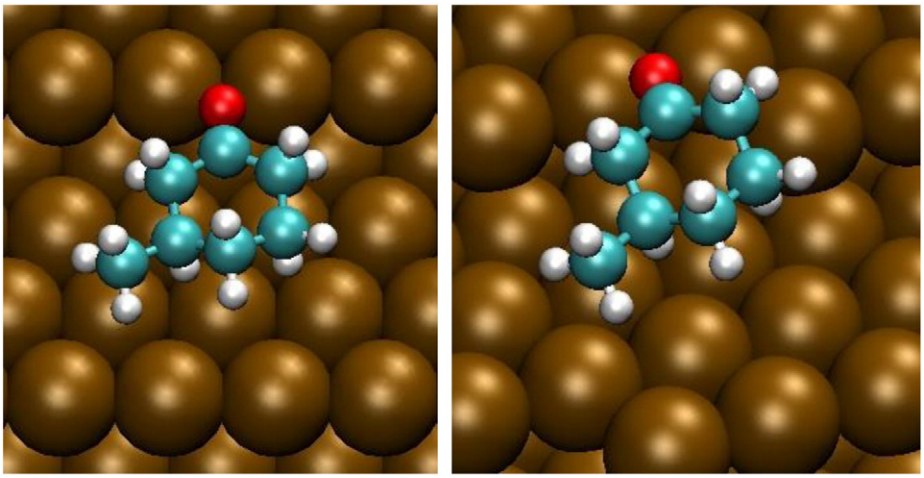

Fig. 3. Adsorption geometry of R-3MCHO on Cu(221) (left) and Cu(643)^R (right), as calculated with DFT using PBE-D2.

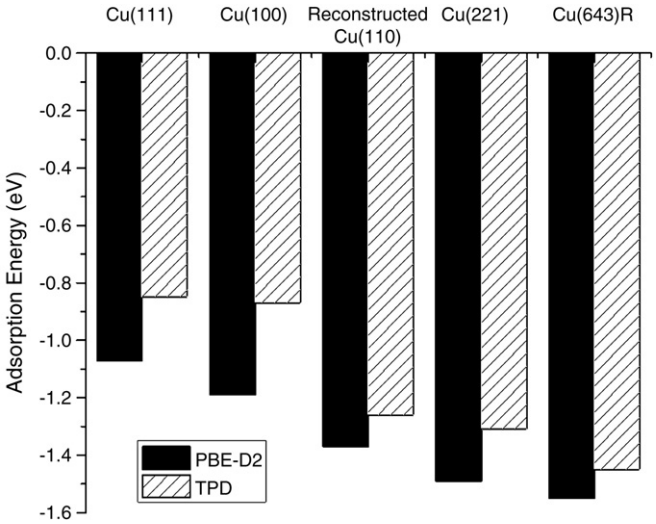

Fig. 5. Adsorption energy of the most preferred configurations of R-3MCHO on the different Cu surfaces.

However, a qualitative agreement between PBE-D2 and TPD results was observed for adsorption energy differences between R-3MCHO adsorption on Cu(111), Cu(221), and Cu(643)^R. Comparison among the three low Miller index Cu surfaces had shown a discrepancy between TPD observations and DFT calculations for Cu(110). DFT calculation employing the (2×1) missing row reconstructed Cu(110) was able to reduce this discrepancy pointing to a possible surface reconstruction.

Acknowledgment

This work has been supported by the National Science Foundation through a collaborative grant CHE-1012358 (B.M., A.J.G.) and CHE-1012524 (D.W., D.S.S.).

References

[1] S. Grimme, WIREs Comput. Mol. Sci. 1 (2011) 211.
[2] J. Klimes, A. Michaelides, J. Chem. Phys. 137 (2012).
[3] S. Grimme, R. Huenerbein, S. Ehrlich, ChemPhysChem 12 (2011) 1258.
[4] J. Klimeš, D.R. Bowler, A. Michaelides, J. Phys. Condens. Matter 22 (2010) 022201.
[5] S. Grimme, J. Comput. Chem. 25 (2004) 1463.
[6] S. Grimme, J. Comput. Chem. 27 (2006) 1787.
[7] M. Dion, H. Rydberg, E. Schröder, D.C. Langreth, B.I. Lundqvist, Phys. Rev. Lett. 92 (2004).
[8] G. Román-Pérez, J. Soler, Phys. Rev. Lett. 103 (2009).
[9] A.D. Becke, J. Chem. Phys. 85 (1986) 7184.
[10] A.D. Becke, J. Chem. Phys. 84 (1986) 4524.
[11] A.D. Becke, Phys. Rev. A 38 (1988) 3098.
[12] J. Klimeš, D. Bowler, A. Michaelides, Phys. Rev. B 83 (2011).
[13] S. Grimme, J. Antony, S. Ehrlich, H. Krieg, J. Chem. Phys. 132 (2010) 154104.
[14] J.-D. Chai, M. Head-Gordon, Phys. Chem. Chem. Phys. 10 (2008) 6615.
[15] A. Gulans, M.J. Puska, R.M. Nieminen, Phys. Rev. B 79 (2009).
[16] J. Wellendorff, A. Kelkkanen, J.J. Mortensen, B.I. Lundqvist, T. Bligaard, Top. Catal. 53 (2010) 378.
[17] B. Liu, L. Cheng, L. Curtiss, J. Greeley, Surf. Sci. 622 (2014) 51.
[18] R. Peköz, K. Johnston, D. Donadio, J. Phys. Chem. C 116 (2012) 20409.
[19] K. Tonigold, A. Gross, J. Chem. Phys. 132 (2010).
[20] R. Hazen, D. Sholl, Nature 2 (2003) 367.
[21] D.S. Sholl, A.J. Gellman, AIChE J 55 (2009) 2484.
[22] P. Szabelski, Physica A 387 (2008) 4615.
[23] P. Szabelski, Chem. Eur. J. 14 (2008) 8312.
[24] F. Zaera, J. Phys. Chem. C 112 (2008) 16196.
[25] J. Horvath, A.J. Gellman, J. Am. Chem. Soc. 124 (2001) 2384.
[26] J.D. Horvath, A. Koritnik, P. Kamakoti, D.S. Sholl, A.J. Gellman, J. Am. Chem. Soc. 126 (2004) 14988.
[27] J.D. Horvath, L. Baker, A.J. Gellman, J. Phys. Chem. C 112 (2008) 7.
[28] Y. Huang, A.J. Gellman, Catal. Lett. 125 (2008) 177.
[29] X. Zhao, J. Am. Chem. Soc. 122 (2000) 12584.
[30] A. Baber, A.J. Gellman, D. Sholl, E. Sykes, J. Phys. Chem. C 112 (2008) 11086.
[31] J.W. Han, J.R. Kitchin, D.S. Sholl, J. Chem. Phys. 130 (2009) 124710.
[32] D. Sholl, A. Asthagiri, T. Power, J. Phys. Chem. B 105 (2001) 4771.
[33] B. Bhatia, D.S. Sholl, J. Chem. Phys. 128 (2008) 144709.
[34] E.R. McNellis, J. Meyer, K. Reuter, Phys. Rev. B 80 (2009) 205414.
[35] K. Fosser, R. Nuzzo, P. Bagus, C. Woll, Angew. Chem. Int. Ed. 41 (2002) 1735.
[36] M. Xi, M.X. Yang, S.K. Jo, B.E. Bent, P. Stevens, J. Chem. Phys. 101 (1994) 9122.
[37] G. Kresse, J. Hafner, Phys. Rev. B 47 (1993) 558.
[38] G. Kresse, J. Hafner, Phys. Rev. B 49 (1994) 14251.
[39] G. Kresse, J. Furthmuller, Comput. Mater. Sci. 6 (1996) 15.
[40] G. Kresse, J. Furthmuller, Phys. Rev. B 54 (1996) 11169.
[41] J.P. Perdew, K. Burke, Y. Wang, Phys. Rev. B 54 (1996) 16533.
[42] J.P. Perdew, K. Burke, M. Ernzerhof, Phys. Rev. Lett. 78 (1997) (1396-1396).
[43] P.E. Blochl, Phys. Rev. B 50 (1994) 17953.
[44] G. Kresse, D. Joubert, Phys. Rev. B 59 (1999) 1758.
[45] H.P. Bonzel, R. Ku, J. Vac. Sci. Technol. 9 (1972) 663.
[46] D.L. Adams, H.B. Nielsen, M.A. Van Hove, A. Ignatiev, Surf. Sci. 104 (1981) 47.
[47] H. Niehus, Surf. Sci. 145 (1984) 407.
[48] J.D. Horvath, A.J. Gellman, J. Am. Chem. Soc. 124 (2002) 2384.
[49] Y. Huang, A.J. Gellman, Top. Catal. 54 (2011) 1403.
[50] A.J. Gellman, J.D. Horvath, M.T. Buelow, J. Mol. Catal. A Chem. 167 (2001) 3.
[51] J.D. Horvath, A.J. Gellman, Top. Catal. 25 (2003) 9.
[52] S.J. Jenkins, S.J. Pratt, Surf. Sci. Rep. 62 (2007) 373.
[53] M.A. van Hove, G.A. Somorjai, Surf. Sci. 92 (1980) 489.
[54] P. Redhead, Vacuum 12 (1962) 203.
[55] R.Z. Lei, A.J. Gellman, B.E. Koel, Surf. Sci. 554 (2004) 125.
[56] G. Witte, S. Lukas, P.S. Bagus, C. Wöll, Appl. Phys. Lett. 87 (2005).
[57] X. Zhao, S.S. Perry, J. Horvath, A.J. Gellman, Surf. Sci. 563 (2004) 217.
[58] D.W. Blakely, G.A. Somorjai, Surf. Sci. 65 (1977) 419.
[59] R. Raval, S. Haq, M.A. Harrison, G. Blyholder, D.A. King, Chem. Phys. Lett. 167 (1990) 391.